Hindawi
International Journal of Differential Equations
Volume 2023, Article ID 5495140, 17 pages
https://doi.org/10.1155/2023/5495140

*Research Article*

# Numerical Investigation of MHD Carreau Nanofluid Flow with Nonlinear Thermal Radiation and Joule Heating by Employing Darcy–Forchheimer Effect over a Stretching Porous Medium

**Endale Ersino Bafe, Mitiku Daba Firdi, and Lemi Guta Enyadene**

*Department of Applied Mathematics, Adama Science and Technology University, Adama, Ethiopia*

Correspondence should be addressed to Endale Ersino Bafe; endaleer@gmail.com

Received 18 April 2023; Revised 1 June 2023; Accepted 28 September 2023; Published 9 October 2023

Academic Editor: Davood D. Ganji



Heat transfer in fluid mechanisms has a stronghold in everyday activities. To this end, nanofluids take a leading position in the advent of the betterment of thermal conductivity. The present study examines numerical investigations of incompressible magnetohydrodynamic (MHD) flow of Carreau nanofluid by considering nonlinear thermal radiation, Joule heating, temperature-dependent heat source/sink, and chemical reactions with attached Brownian movement and thermophoresis above a stretching sheet that saturates the porous medium. Pertaining similarity assumptions are used to change the flow equations into tractable forms of higher order nonlinear ordinary differential equations (ODEs). The continuation technique is adopted in the MATLAB bvp4c package for the numerical outcomes. The velocity, temperature, and nanoparticle concentration distributions in contrast to the leading parameters are availed in graphical and tabular descriptions. Among the many outcomes, increasing the radiation parameter from 0.2 to 0.8 surged the heat transfer rate by 47.78% at $n = 1.5$ and lifted it only by 8.5% at $n = 0.5$. By boosting the magnetic parameter from 0 to 1.5, respective 37.64% and 20.17% rises in local drag forces are achieved in shear-thickening and thinning regions. On top of that, chemical reactions and Brownian motion parameters decay the concentration field. The distinctiveness of this method is that a solution is secured for the problem, which is highly sensitive to initial and boundary conditions. It will be worth mentioning that these fluid flow models will be applicable in various fields, such as engineering, petroleum, nuclear safety processes, and medical science.

## 1. Introduction

Despite their complex stress-strain relationships, in recent years, non-Newtonian fluids have attracted researchers' attention on account of their multidisciplinary applications (see Ref. [1–4]). Non-Newtonian fluids are abundant in several engineering, industrial, and biological activities, such as in food processing, in arterial blood flow, in mud-drilling machines, in polymer suspensions, and in heavy oil lubrications. The notion of improving the thermal conductivity of nanofluids by dispersing nanoparticles in conventional fluids was first initiated by Choi and Eastmann [5]. Nanofluids stand for a mixture of nanosized particles (e.g., Cu, Ti, $Al_2O_3$, and $TiO_2$ normally with size $< 100$ nm) scattered stably in host fluids (e.g., water, blood, ethylene glycol, and vegetable oil). As compared to host fluids, nanofluids possess advanced thermophysical properties. Such fluids being enhanced heat transfer agents, their applications extend to cancer and hyperthermia treatment, solar energy collectors, safety management in nuclear reactors, and cooling processes of electronics, computer chips, and transformers. However, the study of nanofluid is still not at its end, and it seems there is still a need to have an outweighing theory on how to prepare and use nanoparticles to culminate the efficiency of thermal conductivity. A nonuniform heat source/sink in the form of surface temperature and wall heat flux was considered by Ramesh et al. [6] to investigate the stagnation point flow of MHD non-Newtonian dusty fluid flow. Growth in fluid-particle interaction parameter improves the velocity field of dusty fluid and diminishes this distribution for clean fluid as discussed by the authors. Bouslimi et al. [7] used the Runge–Kutta-based shooting method to investigate heat and mass transfer properties of mixed convection nanofluid under Soret diffusion and nonlinear heating caused by an extending surface. The thermal behavior of a hybrid nanofluid in a double-pipe heat exchanger was tested by Jalili et al. [8]. The result indicated that water/$Al_2O_3$ nanofluid has superior convective heat transfer than water/$TiO_2$ nanofluid and pure water. They also found that raising nanofluid concentration from 0.4% to 6% increased the heat transfer rate by 12%. The use of nanoparticles is also an attractive and promising field in the development of diagnostics and treatments for cardiovascular disease. The authors in [9] examined the stenosed artery heat transfer behavior of hybrid nanofluid in a slanted orientation. Stenosis is a condition that results from the narrowing of blood vessels due to the buildup of cholesterol or any other plaque that blocks the smooth flow of blood in the artery. Enhancing the $Al_2O_3$ nanoparticle volume fraction decreases the value of the temperature profile, as elaborated in their work. Additional studies involving the importance of nanofluids can be taken care of through the investigations in [10–13].

Magnetohydrodynamic (MHD) explains the study of dynamic interactions between magnetic fields and conducting fluids. An opposing electric current is induced owing to liquid motion, which alters mechanical properties of the fluid. MHD analysis regulates many natural phenomena and engineering and industrial problems on almost every scale, such as the formation of stars, proper mixing of alloying parts, electrolysis process, the MHD generator, and magnetic filtration and separation. Ishak et al. [14] studied hydromagnetic flow and the transfer of heat energy above a vertical and expanding surface with a varying magnetic field. They noticed that strengthening magnetic intensity brings a reduction of heat energy loss and local skin friction. The accounts of heat source/sink, chemical reaction, and nonlinear thermal radiation on the magnetohydrodynamic flow of Williamson nanofluid was explored by Bouslimi et al. [15]. Their result verified that the heat transfer rate of Williamson nanofluid is adversely affected by rising values of temperature ratios, thermal radiation, and heat generation/absorption parameters.

As a result of the diversity of flow in nature, investigators have recommended various non-Newtonian models based on their constitutive rheological variables, such as Casson fluid, power-law fluid, Williamson fluid, Oldroyd-B fluid, Maxwell fluid, Carreau fluid, and Eyring–Powell fluid. Among these models are Carreau fluids, which are realized as generalized Newtonian fluids having Newtonian ($n = 1$), shear-thickening (or dilatant with $n > 1$), and shear-thinning (or pseudoplastic with $0 < n < 1$) characteristics, where $n$ stands for the power-law index. Examples of these fluids are detergents, fluid crystals, pulps, blood, and synovial fluids. Carreau fluids have gained awareness on account of their importance in the extrusion of polymers, tumor therapy, cosmetics, capillary electrophoresis, and petrochemical industries. The impact of melting and heat source/sink has been analyzed by Khan et al. [16], taking the Carreau nanofluid over a wedge. They recognized that the rise in the above parameters deteriorates the nanoparticle concentration curve in both shear-thinning and thickening regions. The Haar wavelet quasilinearization approach was utilized by Che Ghani and Siri [17], in contemplating the MHD Carreau nanofluid model with the impact of velocity slip boundary and suction/injection above an expanding surface. Babu et al. [18] depicted the nonlinear MHD convective Carreau nanofluid flow with the effect of viscous dissipation and Arrhenius activation energy above an exponentially expanding surface. Many other studies of Carreau nanofluids are detailed in [19–22].

According to Buongiorno's [23] inspection, there exist various slip mechanisms in nanoparticle-based fluid interactions. He identified in the laminar flow region that the prominent dissipative energy sources associated with a nanoparticle-based fluid slip are Brownian motion and thermophoretic diffusion. Contemplating the Rayleigh–Benard problem, the impact of thermophoresis and Brownian movement on CuO-water nanofluid heat transfer nature was studied by Haddad et al. [24]. Their study revealed the influence of thermophoresis and Brownian motion is more amplified at low-volume fractions of nanoparticles. The influence of thermophoretic diffusion and Brownian movement on the mixed convection flow of Carreau nanofluid was studied by Irfan [25]. The importance of thermophoretic and Brownian diffusion on MHD nanofluid flow over a stretching circular cylinder with the insertion of a variable magnetic field, free stream velocity, and multiple slips was examined by Majeed et al. [26]. Thermal analysis on the effect of thermophoresis, Brownian motion, and Hall currents in micropolar nanofluids was presented by Jalili et al. [27]. Lately, the authors in [28] considered the flow behavior of micropolar nanofluid subjected to electromagnetism, thermophoresis, and Brownian motion in a rotating realm. Further investigations on Brownian diffusion and thermophoresis in light of various non-Newtonian fluids can be addressed in [29–31].

Many scientists are motivated to understand heat and mass transfer phenomena associated with chemical reactions and chemical transportation processes by considering their industrial applications in combustion, catalysis, and biochemical systems. These chemically reacting systems involve homogeneous (or bulk) and heterogeneous (or surface) reactions. Representing homogeneous reactions by cubic autocatalysis and heterogeneous reactions by a first-order process, Merkin [32] studied the boundary-layer flow of homogeneous-heterogeneous reactions. The author has indicated that the surface reaction is the most influential mechanism near the front edge of a uniform stream flow over a flat surface. In [33], Khan et al. picked the MHD flow of the Powell–Eyring fluid model to elaborate on the Newtonian heating impact on homogeneous and heterogeneous reactions. They observed that the skin friction coefficient advances for large values of magnetic and fluid parameters. In contrast, the mass transfer rate dampens for a homogeneous reaction parameter. Additional furtherance on chemical reactions for various non-Newtonian fluids is reported in [34–37].

High-temperature gradient MHD convective flow problems are remarkably influenced by thermal radiation. Its significance can be seen in nuclear power plants, electrical power generators, solar power collectors, glass-blowing, and manufacturing of plastic and rubber sheets. To analyze the energy production feature of flow between two circular plates, Jalili et al. [38] studied the thermal radiation influence of unsteady compressing flow of magnetohydrodynamic Casson fluid. They identified that non-Newtonian fluid temperature improves by 20%, responding to a surge in the squeezing factor value. In light of the 2D cavity and 3D cavity, the impact of magnetic field and thermal radiation on the transport process of magnetohydrodynamic convection flow was exploited by Zhang et al. [39]. The study unfolded when strong thermal radiation and weak magnetic field are set forth, and the difference in flow and thermal radiation between 2D and 3D cavities is notable as compared to weak thermal radiation and strong magnetic field combination effects. Shaw et al. [40] investigated MHD hybrid nanofluid flow exposed to quadratic and nonlinear thermal radiations. By considering radiation properties and convective phenomena, the influence of Joule heating on magnetic Carreau nanofluid has been explored in [41]. Recently, employing hybrid analytical and numerical techniques, the authors in [42] presented the heat and mass transport features of axisymmetric micropolar fluid constricted to the magnetic field in a cylindrical polar system. Their work showed that increasing the radiation parameter from 0 to 8% changes the shape of the temperature profile while keeping the maximum and minimum temperatures unaltered.

The transport process of non-Newtonian fluid via porous media is an attractive area of research owing to its vast applications, such as packed bed reactors, geothermal industries, enhanced oil recovery, drying of paper pulp, gel chromatography, and soil structures. A pioneering work regarding the flow of fluid in a porous medium was initiated by Darcy in 1856. A mixed convection power-law fluid flow drenching the porous space was discussed by authors in [43]. The nanofluid flow in a Darcy–Forchheimer porous medium was studied by Rasool and Zhang [44], taking into account the Cattaneo–Christov heat and mass flux model. They disclosed that resistive force resulting from the porosity factor increases the temperature field. Conversely, the concentration field of nanoparticles decays in response to an increase in the inertial force. The effect of using different hybrid nanofluids as solar energy absorbers in a Darcy–Forchheimer porous medium was studied by Alzahrani et al. [45]. The account of the non-Darcy–Forchheimer law on MHD Carreau fluid flow subjected to a heat source/sink and thermal radiation above a stretching sheet was anticipated by Siddiq et al. [46].

We have surveyed the above literature and many more not listed here and found that there does not exist a study that demonstrates the combined impacts of nonlinear thermal radiation, Ohmic heating, heat source/sink, chemical reaction, and Darcy–Forchheimer inertial effect on MHD flow of Carreau nanofluid embedding linearly stretching porous surface with Brownian motion and thermophoretic events.

## 2. Problem Formulation

The mathematical model of the present study is developed by assuming a steady, 2D, viscous, and incompressible nonlinear radiative flow of magneto Carreau nanofluid above a stretching sheet. The sheet is expanding with the velocity $u_w = a_0 x$, where $a_0$ is a stretching constant. A constant magnetic intensity $B_0$ is administered orthogonal to the surface. We suppose a small magnetic Reynolds number in order to detach the influence of the induced magnetic field. Furthermore, the effects of Hall current and ion slip are ignored. The porous sheet is kept at a temperature $T_w$, and the fluid's free stream temperature is $T_\infty$ with $T_w > T_\infty$. The $x$-axis is aligned in the direction of extension of the sheet, while the $y$-axis is normal to it. The physical sketch of the flow is represented in Figure 1.

The Cauchy stress tensor $\boldsymbol{\tau}$ for Carreau model rheology and its corresponding shear rate $\gamma'$ are premeditated as follows (see [47–49]):

$$\boldsymbol{\tau} = -p\mathbf{I} + \mu \mathbf{A}_1, \tag{1}$$

$$\mu = \mu_\infty + \left(\mu_0 - \mu_\infty\right)\left(1 + (\lambda\dot{\gamma})^2\right)^{(n-1/2)}, \tag{2}$$

$$\gamma' = \sqrt{\frac{1}{2}\sum_i \sum_j \gamma'_{ij}\gamma'_{ji}} = \sqrt{\frac{1}{2}\operatorname{tr}\left(\mathbf{A}_1^2\right)}. \tag{3}$$

Here, $\mathbf{I}$, $p$, $\mu_\infty$, $\mu_0$, $\mathbf{A}_1 = (\text{gradV}) + (\text{gradV})^T$, $n$, and $\lambda$ denote the identity tensor, pressure, infinite shear rate viscosity, zero-shear rate viscosity, first Rivlin–Ericksen tensor, power-law index, and time material parameter, respectively.

In two-dimensional steady flow, the velocity, temperature, and concentration fields take the following form:

$$\mathbf{V} = [u(x,y), v(x,y)], T = T(x,y), C = C(x,y), \tag{4}$$

where $u$ and $v$ represent the respective $x$-and $y$-direction velocities.

Depending on the above assumptions, we execute the boundary-layer analysis that leads us to the set of equations governing the conservation of continuity, momentum, energy, and nanoparticle concentration expressed, respectively, as follows:

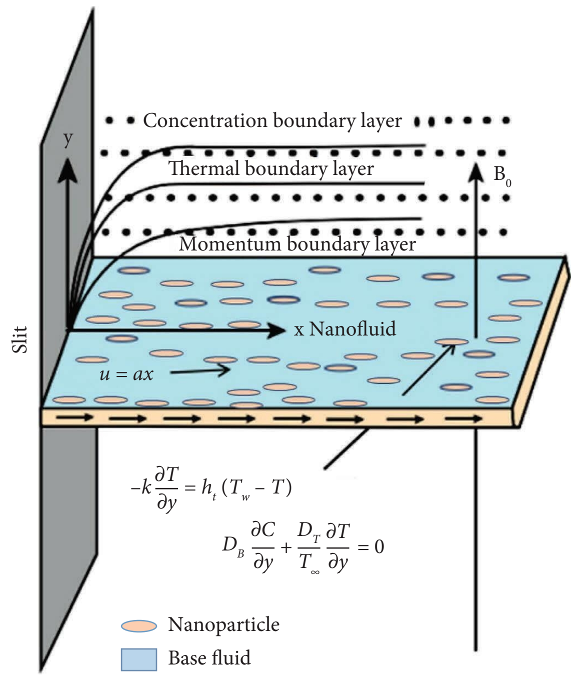


Figure 1: Geometry of the flow problem.

$$\frac{\partial u}{\partial x} + \frac{\partial v}{\partial y} = 0, \tag{5}$$

$$\begin{aligned} u\frac{\partial u}{\partial x} + v\frac{\partial u}{\partial y} &= \nu\frac{\partial^2 u}{\partial y^2}\left[1 + \lambda^2\left(\frac{\partial u}{\partial y}\right)^2\right]^{n-1/2} \\ &\quad + \nu(n-1)\lambda^2\frac{\partial^2 u}{\partial y^2}\left(\frac{\partial u}{\partial y}\right)^2\left[1 + \lambda^2\left(\frac{\partial u}{\partial y}\right)^2\right]^{n-3/2} \\ &\quad - \frac{\sigma B_0^2}{\rho}u - \frac{\mu\beta_1}{\rho p_m}u - \frac{f_c\beta_1}{\sqrt{p_m}}u^2, \end{aligned} \tag{6}$$

$$\begin{aligned} u\frac{\partial T}{\partial x} + v\frac{\partial T}{\partial y} &= \frac{k}{\rho c_p}\frac{\partial^2 T}{\partial y^2} + \frac{\sigma B_0^2}{\rho c_p}u^2 + \tau D_B\left(\frac{\partial T}{\partial y}\frac{\partial C}{\partial y}\right) \\ &\quad + \frac{\tau D_T}{T_\infty}\left(\frac{\partial T}{\partial y}\right)^2 - \frac{1}{\rho c_p}\frac{\partial q_r}{\partial y} + \frac{Q_a}{\rho c_p}(T - T_\infty), \end{aligned} \tag{7}$$

$$u\frac{\partial C}{\partial x} + v\frac{\partial C}{\partial y} = D_B\frac{\partial^2 C}{\partial y^2} + \frac{D_T}{T_\infty}\left(\frac{\partial^2 T}{\partial y^2}\right) - k_0(C - C_\infty). \tag{8}$$

Here, $\tau = ((\rho c_p)_p/(\rho c_p)_f)$ denotes the effective heat capacity ratio of nanoparticles to base fluid. All the other notations are indicated in nomenclature. As in [17], the boundary conditions suitable for the current problem are as follows:

$$\begin{aligned} &u = u_w = a_0 x, v = v_w, -k\frac{\partial T}{\partial y} = h_t(T_w - T), \\ &D_B\frac{\partial C}{\partial y} + \frac{D_T}{T_\infty}\frac{\partial T}{\partial y} = 0 \text{ at } y = 0, \\ &u \longrightarrow 0, v \longrightarrow 0, T \longrightarrow T_\infty, C \longrightarrow C_\infty \text{ as } y \longrightarrow \infty, \end{aligned} \tag{9}$$

where $v_w, h_t, T_w$ are the mass transfer velocity, heat transfer coefficient, and wall temperature of the fluid, respectively.

For an optically thick medium, the Rosseland approximation for the radiative heat flux provides

$$q_r = \frac{-4\sigma^*}{3k_e}\frac{\partial T^4}{\partial y}, \tag{10}$$

where $k_e$ is the coefficient of the mean absorption and $\sigma^*$ is the Stefan–Boltzmann constant. For nonlinear radiation,

$$q_r = \frac{-4\sigma^*}{3k_e}\frac{\partial T^4}{\partial y} = \frac{-16\sigma^*}{3k_e}T^3\frac{\partial T}{\partial y}. \tag{11}$$

We adopt the following similarity transformations:

$$\begin{aligned} &\eta = y\sqrt{\frac{u_w}{\nu x}}, \psi = \sqrt{\nu u_w x}\, f(\eta), \theta(\eta) = \frac{T - T_\infty}{T_w - T_\infty}, \\ &\phi(\eta) = \frac{C - C_\infty}{C_w - C_\infty}, \theta_w = \frac{T_w}{T_\infty}, \end{aligned} \tag{12}$$

where $\eta$ is the similarity variable and $\psi(x, y)$ denotes the stream function satisfying the equation of continuity $u = \partial\psi/\partial y$, $v = -\partial\psi/\partial x$.

Using equations (1)–(3), (11), and (12), the transformed nondimensional form of governing equations (5)–(8) and corresponding boundary conditions (9) are expressed as follows:

$$\left[1 + nw_e^2 f''^2\right]\left[1 + w_e^2 f''^2\right]^{n-3/2} f''' + ff'' - f'^2 - M^2 f' - Pf' - \alpha f'^2 = 0, \tag{13}$$

$$\begin{aligned} &\theta'' + R_d[1 + (\theta_w - 1)\theta]^3\theta'' + 3R_d(\theta_w - 1)[1 + (\theta_w - 1)\theta]^2\theta'^2 + \Pr EcM^2 f'^2 \\ &\quad + \Pr f\theta' + \Pr N_b\theta'\phi' + \Pr\omega\theta + \Pr N_t\left(\theta'\right)^2 = 0, \end{aligned} \tag{14}$$

$$\phi'' + Scf\phi' + \frac{N_t}{N_b}\theta'' - Sc\gamma\phi = 0. \tag{15}$$

With the boundary conditions,

$$\begin{aligned} &f(\eta) = S, f'(\eta) = 1, \theta'(\eta) = -\zeta_1(1 - \theta(\eta)), \\ &N_b\phi'(\eta) + N_t\theta'(\eta) = 0, \text{at } \eta = 0, \\ &f' \longrightarrow 0, \theta \longrightarrow 0, \phi \longrightarrow 0 \text{ as } \eta \longrightarrow \infty, \end{aligned} \tag{16}$$

where $W_e^2 = a_0^3\lambda^2x^2/\nu$ is the Weissenberg number, $p_r = \nu\rho c_p/k$ is the Prandtl number, $P = \nu\beta_1/p_m a_0$ is the porosity parameter, $\alpha = f_c\beta_1 x/\sqrt{p_m}$ is the local inertia coefficient parameter, $E_c = u_w^2/c_p(T_w - T_\infty)$ is the Eckert number, $M = \sqrt{\sigma_e B_0^2/\rho a_0}$ is the magnetic parameter, $R_d = 16\sigma^\star T_\infty^3/3kk_e$ is the thermal radiation parameter, $\theta_w = T_w/T_\infty$ is the ratio temperature parameter, $N_b = \tau D_B/\nu(C_w - C_\infty)$ is the Brownian motion parameter, $N_t = \tau D_T/\nu T_\infty(T_w - T_\infty)$ is the thermophoresis parameter, $\omega = Q_a/a_0\rho c_p$ is the heat source/sink parameter, $Sc = \nu/D_B$ is the Schmidt number, $\gamma = k_0/a_0$ is the chemical reaction parameter, and $\zeta_1 = -h_t/k\sqrt{\nu/a_0}$ is the Biot number.

## 3. Numerical Approaches

Bvp4c is a residual error-based mesh adaptive finite difference program that executes the three-stage Lobatto IIIa formula. The conventional method in Bvp4c provides a guess to the missed initial conditions. However, we found our problem very sensitive to the initial conditions and boundary values. Therefore, we adopted the continuation technique to resolve this problem. It is a tactic developed by Robert and Shipman [50]. They used the method to solve boundary value problems that cannot be addressed by conventional shooting methods. Introducing variable $\chi_i$ for $i = 1, 2, \ldots 7$, we reduce the order of equations (13)–(15) into a system of 7 ODEs:

$$\begin{cases} f = \chi_1, f' = \chi_2, f'' = \chi_3, f''' = \chi_3', \theta = \chi_4, \\ \theta' = \chi_5, \theta'' = \chi_5', \phi = \chi_6, \phi' = \chi_7, \phi'' = \chi_7'. \end{cases} \tag{17}$$

For numerical computation, we have used the tolerance error, RelTol $= 1e - 8$. Next, to implement the continuation method, the following steps are taken in the Bvp4c MATLAB program:

(1) Using a dummy parameter $\delta$, write the system as a sum of its linear and nonlinear parts

(2) Using normal guess and transformed boundary conditions (19), approximate the solution for (18) by the linear part

(3) Employing computed values of step 2 and taking a small positive fraction of $\delta$ as a coefficient of nonlinear part, approximate the solution

(4) Repeat step 3 with small increment in $\delta$ until we come up with approximate solution to the problem with in the prescribed error tolerance

$$\begin{pmatrix} \chi_1' \\ \chi_2' \\ \chi_3' \\ \chi_4' \\ \chi_5' \\ \chi_6' \\ \chi_7' \end{pmatrix} = \begin{pmatrix} \chi_2 \\ \chi_3 \\ 0 \\ \chi_5 \\ 0 \\ \chi_7 \\ Sc\gamma\chi_6 \end{pmatrix} + \delta \begin{pmatrix} 0 \\ 0 \\ \dfrac{(1+\alpha)\chi_2^2 + \left(M^2+P\right)\chi_2 - \chi_1\chi_3}{\left(1+nW_e^2\chi_3^2\right)\left(1+W_e^2\chi_3^2\right)^{n-3/2}} \\ 0 \\ \dfrac{-3R_d\left(\theta_w-1\right)\left(1+\left(\theta_w-1\right)\chi_4\right)^2\chi_5^2 - P_r\left(EcM^2\chi_2^2 + \chi_1\chi_5 + N_b\chi_5\chi_7 + \omega\chi_4 + N_t\chi_5^2\right)}{\left(1+R_d\left(1+\left(\theta_w-1\right)\chi_4\right)^3\right)} \\ 0 \\ \dfrac{N_t}{N_b}\left(\dfrac{3R_d\left(\theta_w-1\right)\left(1+\left(\theta_w-1\right)\chi_4\right)^2\chi_5^2 + P_r\left(EcM^2\chi_2^2 + \chi_1\chi_5 + N_b\chi_5\chi_7 + \omega\chi_4 + N_t\chi_5^2\right)}{\left(1+R_d\left(1+\left(\theta_w-1\right)\chi_4\right)^3\right)}\right) - Sc\chi_1\chi_7 \end{pmatrix}, \tag{18}$$

$$\begin{cases} \chi_1(0) = S, \chi_2(0) = 1, \chi_5(0) = -\zeta_1\left(1-\chi_4(0)\right), N_b\chi_7(0) + N_t\chi_5(0) = 0 \text{ at } \eta = 0, \\ \chi_2(\eta) \longrightarrow 0, \chi_4(\eta) \longrightarrow 0, \chi_6(\eta) \longrightarrow 0 \text{ as } \eta \longrightarrow \infty. \end{cases} \tag{19}$$

To examine the surface drag force, heat, and mass transfer rate, we have determined the skin friction, Nusselt number, and Sherwood number for Carreau fluid as follows:

$$\begin{aligned} C_{fx} &= \frac{2\tau_w}{\rho u_w^2}, \tau_w = \mu\frac{\partial u}{\partial y}\left[1+\lambda^2\left(\frac{\partial u}{\partial y}\right)^2\right]^{n-1/2}\Bigg|_{y=0}, \\ \mathrm{Nu}_x &= \frac{xq_w}{k\left(T_w - T_\infty\right)}, q_w = -k\frac{\partial T}{\partial y}\bigg|_{y=0} + \left(q_r\right)_w, \\ \mathrm{Sh}_x &= \frac{xm_w}{D_B\left(\mathrm{Cw} - C_\infty\right)}, m_w = -D_B\frac{\partial C}{\partial y}\bigg|_{y=0}. \end{aligned} \tag{20}$$

In a dimensionless form, the local Reynolds number is $\mathrm{Re} = u_w x/\nu$; the local skin friction, Nusselt, and Sherwood number, respectively, take the following form:

$$\begin{aligned} \mathrm{Re}^{1/2}C_{fx} &= -2f''(0)\left[1+W_e^2 f''(0)^2\right]^{n-1/2}, \\ \mathrm{Re}^{-1/2}Nu_x &= -\left(1+R_d\theta_w{}^3\right)\theta'(0), \\ \mathrm{Re}^{-1/2}Sh_x &= -\phi'(0). \end{aligned} \tag{21}$$

## 4. Results and Discussion

The transformed first-order ODE (18), along with the corresponding boundary conditions (19), has been solved using the continuation technique implemented on MATLAB package bvp4c. The influence of leading parameters on dimensionless fluid velocity, temperature, and nanoparticle concentration is discussed for both shearing cases in graphical and tabular forms. For the accuracy and verification of the method, a comparison in local shear stress has been made for the present and published results in [46] under some restricted conditions.

The Lorentz force effect resulting from the presence of applied magnetic field is noticed in Figures 2–4. This force regulates the way of fluid flow. Figure 2 indicates for both dilatant and pseudoplastic fluids, an increase in the magnetic parameter value deteriorates the velocity field. Here, the velocity curve downturn in the latter fluid type is higher than in the former one. Across the boundary layer, a sharp surge in the temperature field is achieved in response to increasing values of M. A similar behavior is noticed in the nanoparticle concentration at the free stream, and it follows the reverse direction near the wall (see Figures 3 and 4). These results coincide with the physical meaning of increasing magnetic field that intensifies the Lorentz force, which in turn has the capability of increasing the nanoparticle volume fraction in the motion of nanofluid and fluid temperature as well. Figures 5–7 illustrate the Weissenberg number ($W_e$) effect. Practically, We measures the time taken by the fluid to relax before regaining its original shape. An increase in $W_e$ amplifies the gap between shear-thinning and thickening regions of velocity, temperature, and concentration fields. Enhancing $W_e$ stimulates velocity in shear-thickening cases and declines it in shear-thinning regions. The opposite scenario is demonstrated in temperature and concentration fields.

The local inertia coefficient and porosity parameter influence on the momentum boundary layer are realized in Figures 8 and 9, respectively. For both regions, strengthening these parameters discouraged momentum thickness.

Temperature distribution responses to porosity, thermophoresis, and temperature ratio parameter values are demonstrated in Figures 10–12. The increment in these parameters augmented the temperature field and its corresponding thermal thickness. The result in Figure 11 agrees with the fact that an increase in the thermophoresis parameter results in extra particles pushing away from the stretchable wall. As a result, the temperature distribution is facilitated. In Figure 12, the improvement of $\theta_w$ initiates the conductivity of the fluid flow. Consequently, $\theta$ uplifts. However, as noticed in the figures, shear-thinning fluids are more influenced than shear-thickening fluids for the mentioned parameters. The behavior of the temperature field corresponding to variations in the Eckert number is captured in Figure 13. The rise in $E_c$ imparts excess viscous heating to the fluid. Following this, kinetic energy is transformed into internal energy, which in turn pushes up the temperature curve. Figures 14–16 display the impacts of other pertinent parameters on temperature boundary layer thickness. Figure 14 describes that $\theta$ decreases with a rise in the value of the Prandtl number in the two fluid regions. Figure 15 shows us that a significant rise in temperature distribution can be achieved by a small increment in the Biot number, $\zeta_1$. The effect of thermal radiation is analyzed in Figure 16. Here, the temperature distribution and its corresponding thermal thickness are escalated by the rise of $R_d$. Substantially, the growth in radiation ray transports more heat energy to the running fluid, and in turn, a rise in thermal boundary layer thickness ensues. Here, we bear in mind that thermal boundary layer thickness is higher in the case of shear thinning than in shear-thickening behavior.

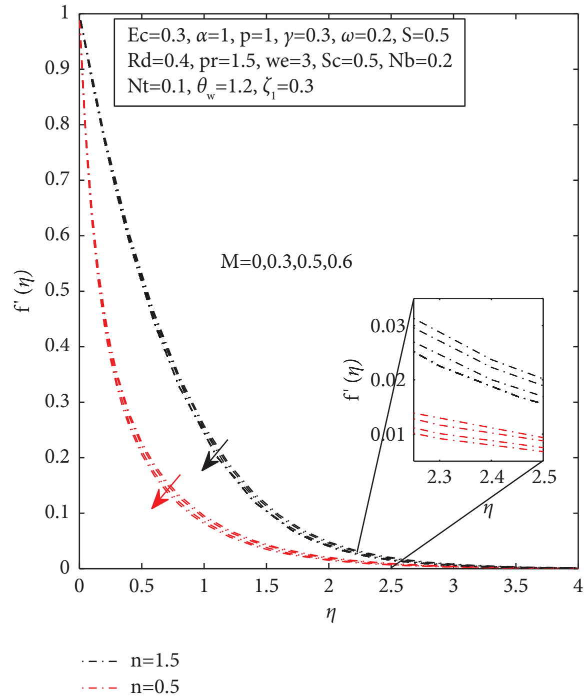


Figure 2: Velocity variations contrasted with $M$.

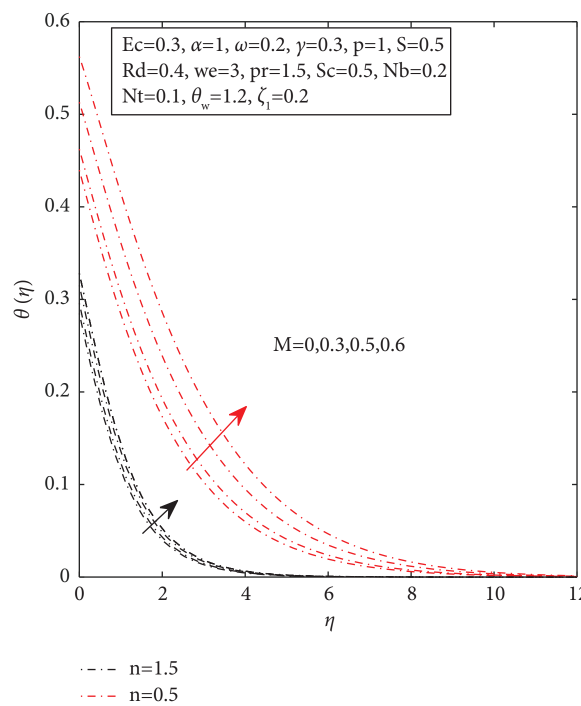


Figure 3: Temperature variations contrasted with $M$.

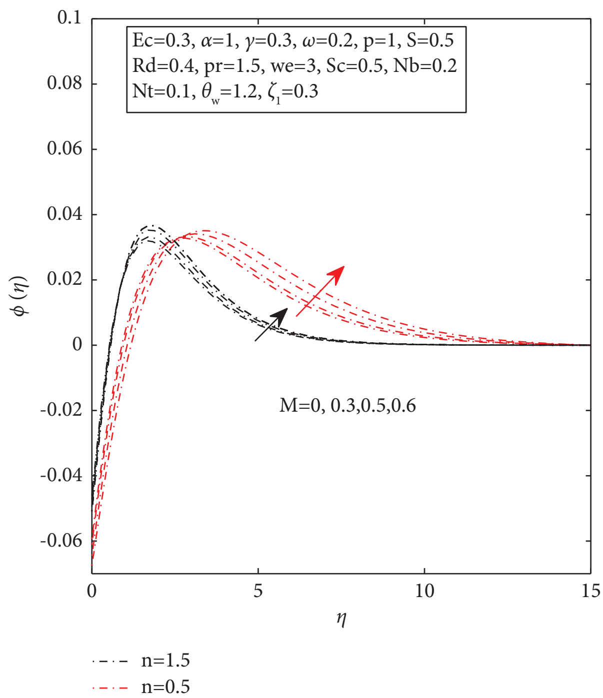


Figure 4: Concentration variations contrasted with $M$.

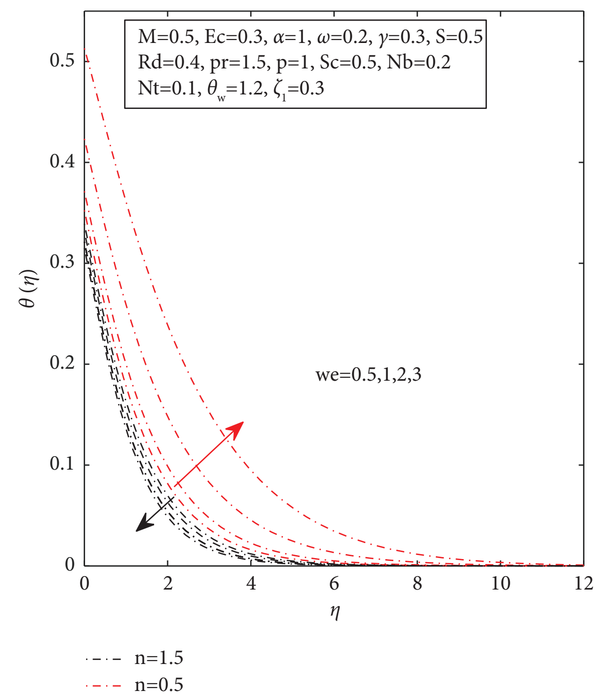


Figure 6: Temperature variations contrasted with $W_e$.

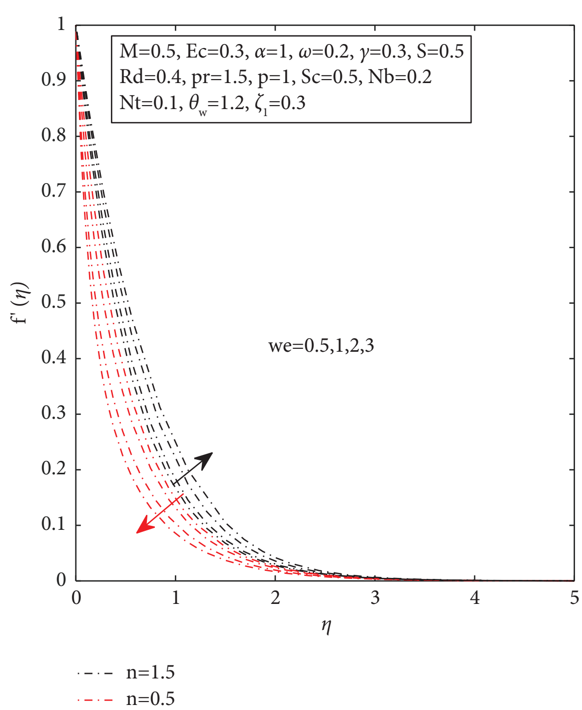


Figure 5: Velocity variations contrasted with $W_e$.

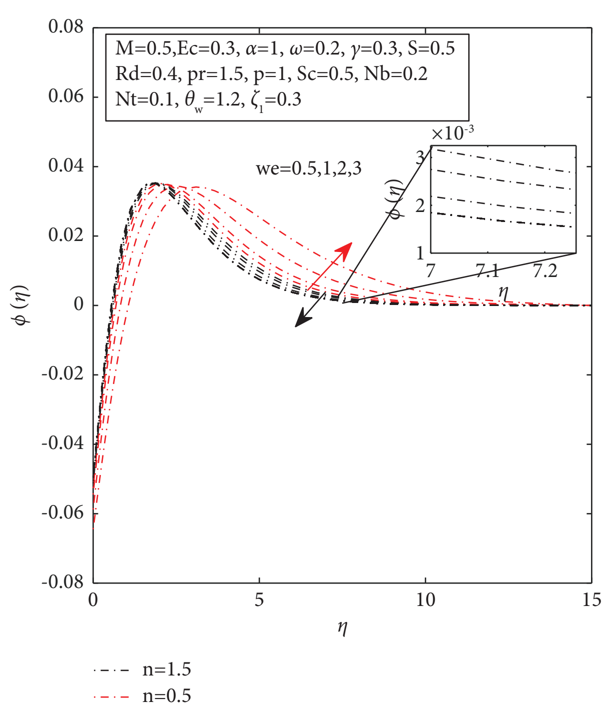


Figure 7: Concentration variations contrasted with $W_e$.

The temperature field response for variations in the heat source/sink parameter is illustrated in Figure 17. The rise in values of $\omega$ causes temperature distribution growth.

Figures 18–20 portray the twofold influence of parameter thermophoresis ($N_t$), Brownian motion ($N_b$), and the Schmidt number ($S_c$) in nanoparticle concentration. Near the wall and in the free stream, their variation brings reversed effects. Figure 18 displays a growing behavior of the concentration field for the rise in $N_t$. Amplifying the thermophoretic parameter causes the microscopic transfer of nanoparticles from warmer to cooler regions, which in turn grows the nanoparticle concentration. An increase in the Brownian motion parameter declines the

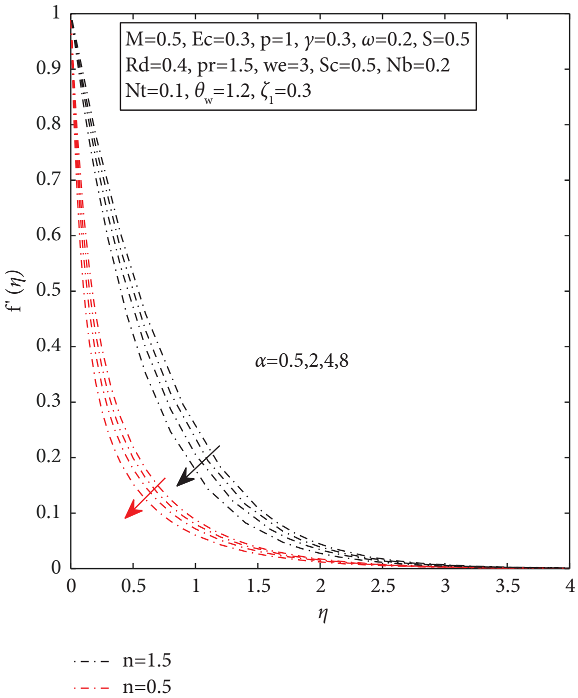


Figure 8: Velocity variations contrasted with $\alpha$.

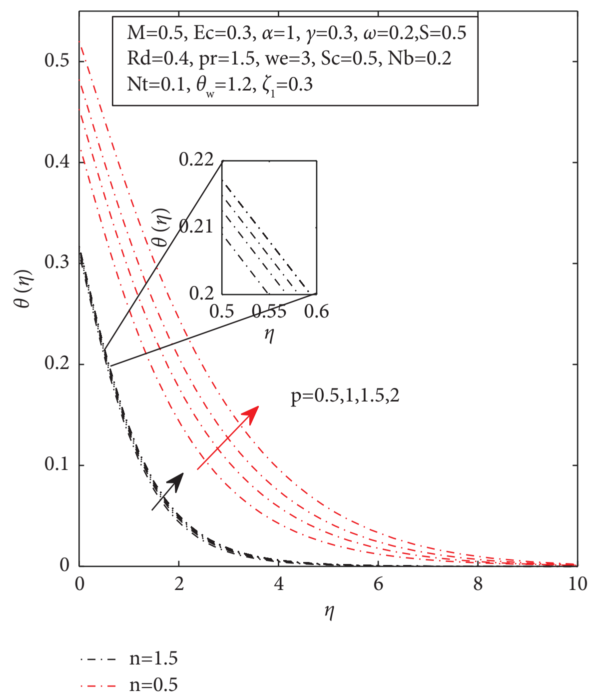


Figure 10: Temperature variations contrasted with $p$.

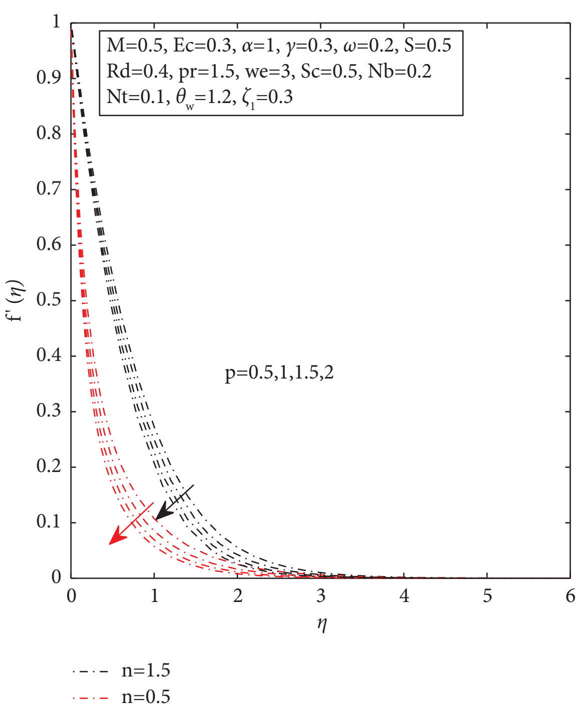


Figure 9: Velocity variations contrasted with $p$.

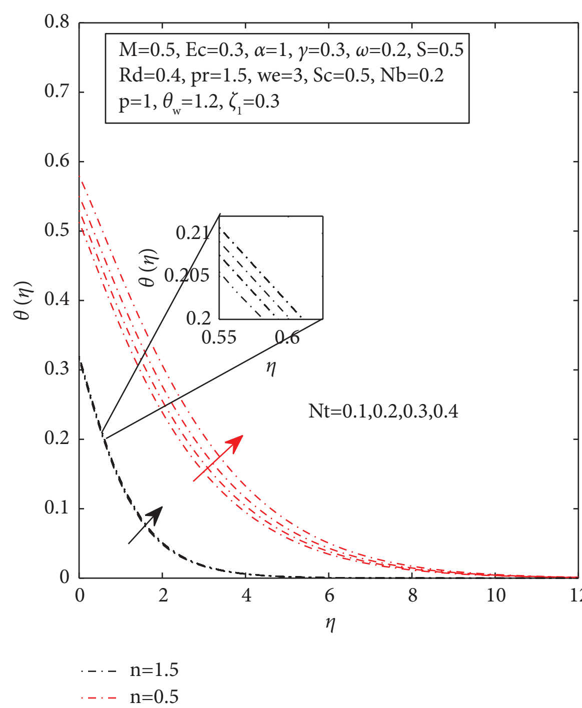


Figure 11: Temperature variations contrasted with $N_t$.

nanoparticle concentration field, as witnessed in Figure 19. Boundary layer diffusion of nanoparticles is strengthened as the value in Brownian parameter surges. Consequently, nanoparticle concentration downturns. Figure 20 shows the expected response of nanoparticle concentration for an increase in the Schmidt number value. The coefficient of mass diffusion is inversely related to the Schmidt number. As a result, a decline in the distribution of nanoparticle concentration and its corresponding solutal thickness is realized. Figure 21 presents the nanoparticle concentration distribution to deliberate the influence of variations of the chemical reaction parameter. It reveals a decaying nature in the nanoparticle concentration field for the rise in $\gamma$.

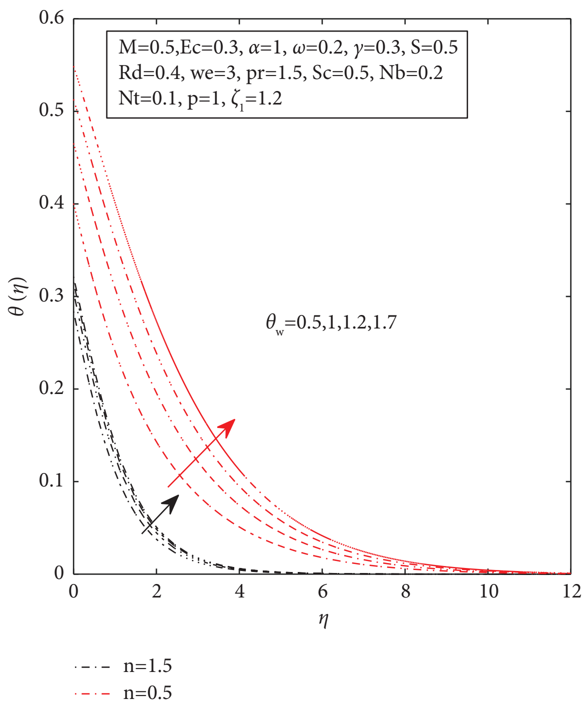


Figure 12: Temperature variations contrasted with $\theta_w$.

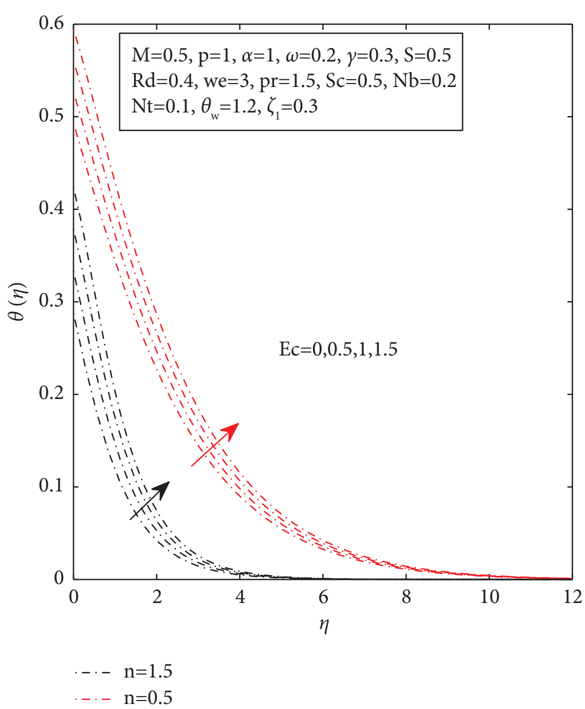


Figure 13: Temperature variations contrasted with $E_c$.

Table 1 compares the shear stress values of the present result with the work of Siddiq et al. [46], under certain restricted conditions. It can be concluded that an excellent agreement is achieved. From Table 1, we notice that increases in parameters $M$, $p$, and $\alpha$ inflated wall shear stress. On the contrary, an increase in $n$ and $W_e$ deflated it.

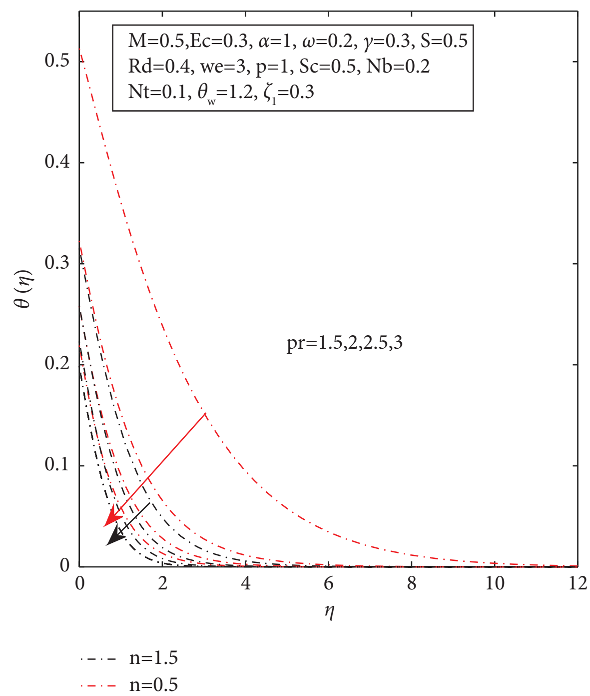


Figure 14: Temperature variations contrasted with $p_r$.

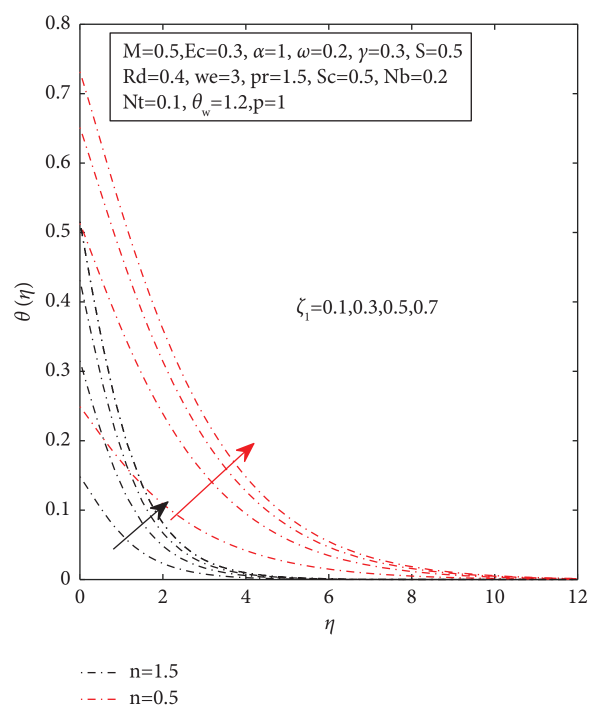


Figure 15: Temperature variations contrasted with $\zeta_1$.

Table 2 executes the local heat transfer rate against various values of listed parameters. Except for the Eckert number, the surge in the heat transfer rate occurred with the rise in parameters $P_r$, $R_d$, $\theta_w$, and $\zeta_1$ for both shear-thinning and thickening behaviors. Here, we perceive that the heat transfer rate in the shear-thickening region is better than in the shear-thinning region.

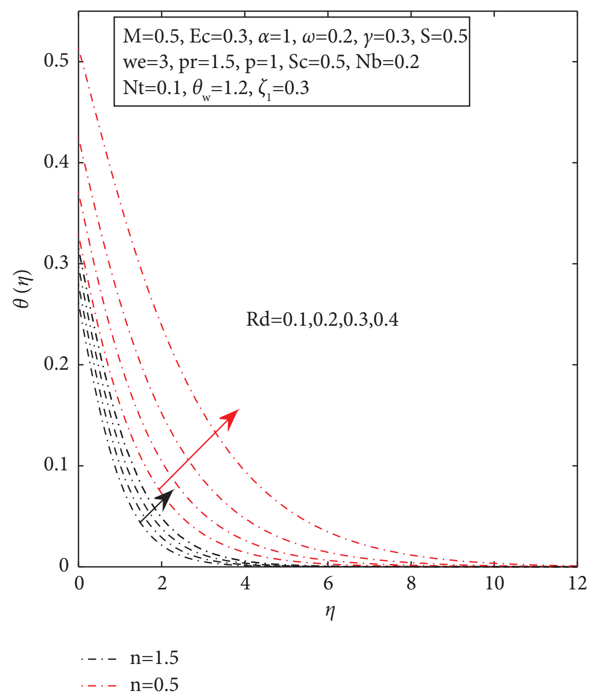


Figure 16: Temperature variations contrasted with $R_d$.

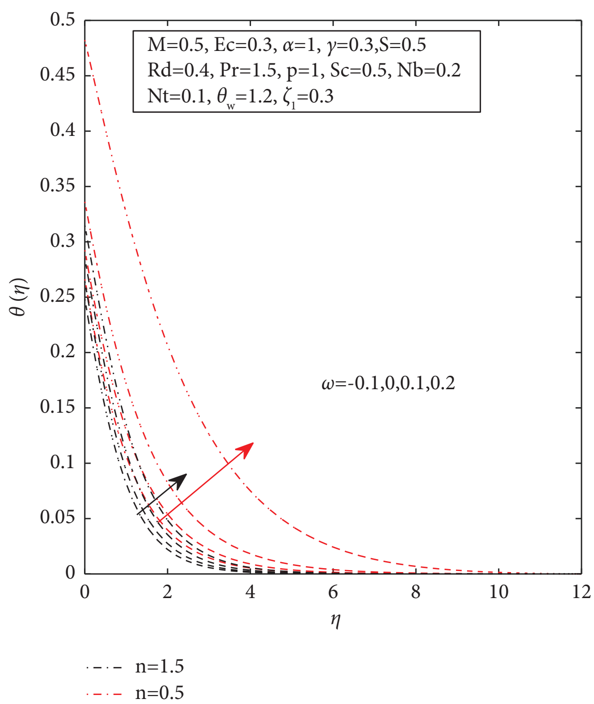


Figure 17: Temperature variations contrasted with $\omega$.

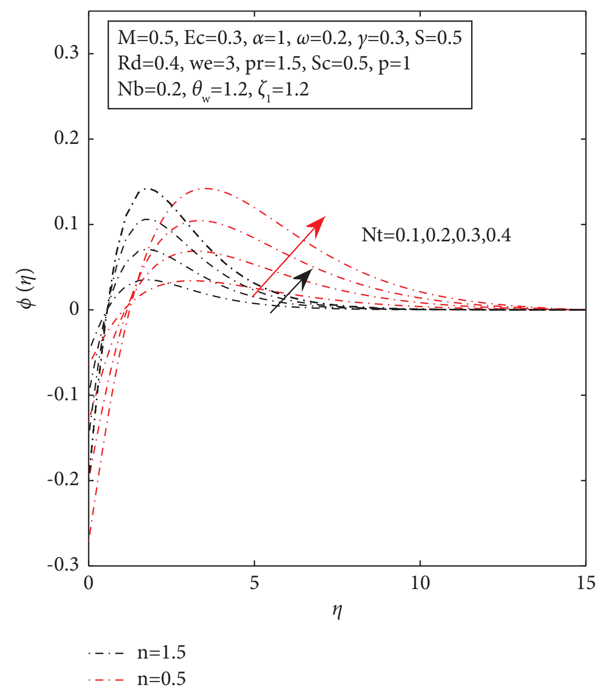


Figure 18: Concentration variations contrasted with $N_t$.

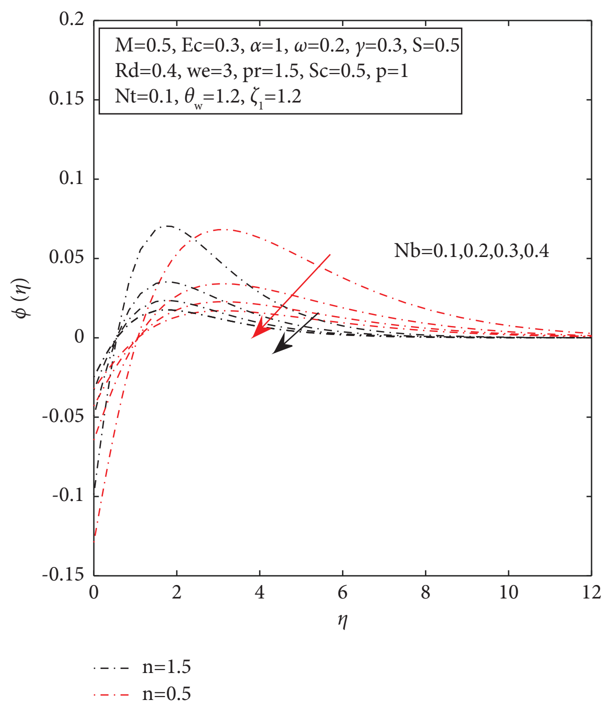


Figure 19: Concentration variations contrasted with $N_b$.

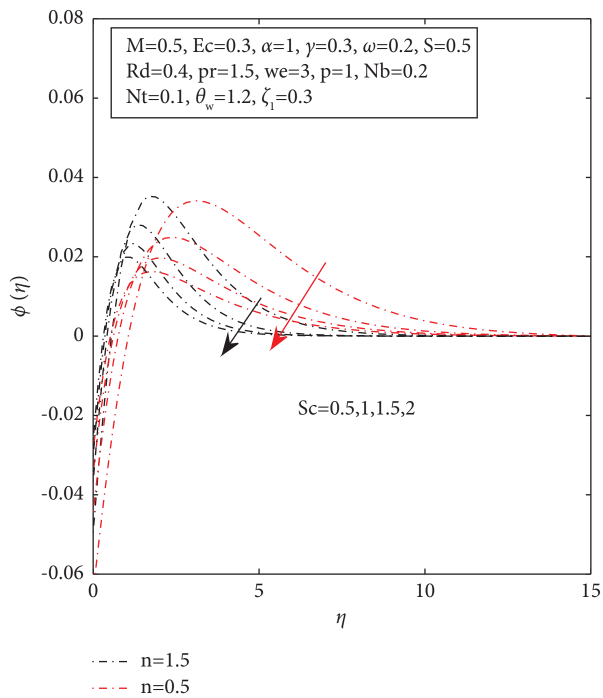


Figure 20: Concentration variations contrasted with Sc.

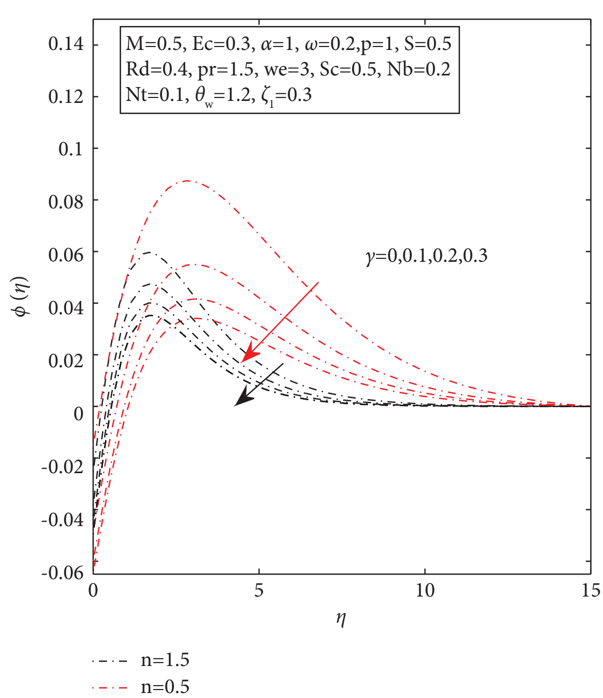


Figure 21: Concentration variations contrasted with $\gamma$.

Table 1: Comparison of shear stress $-f''(0)$ of the present result with the work in [46] for different values of $M$, $p_r$, $\alpha$, $p$, and $W_e$ fixing $\theta_w = 1$, $N_b = N_t = 0.1$.

| Parameters | | | | | $-f''(0)$ | |
|---|---|---|---|---|---|---|
| $M$ | $p$ | $\alpha$ | $n$ | $W_e$ | [46] | $P_r$. result |
| 0 | 1 | 1 | 1.5 | 3 | 1.214344 | 1.214344 |
| 0.7 | | | | | 1.288215 | 1.288216 |
| 1 | | | | | 1.358280 | 1.358280 |
| 1.2 | | | | | 1.414282 | 1.414282 |
| 1.5 | | | | | 1.508864 | 1.508864 |
| 0.5 | 1 | | | | 1.252943 | 1.252945 |
| | 2 | | | | 1.390551 | 1.390552 |
| | 4 | | | | 1.613836 | 1.613836 |
| | 6 | | | | 1.796208 | 1.796208 |
| | 1 | 2 | | | 1.343451 | 1.343452 |
| | | 5 | | | 1.570936 | 1.570939 |
| | | 8 | | | 1.756682 | 1.756685 |
| | | 10 | | | 1.865437 | 1.865442 |
| | | 1 | 0.5 | | 5.340793 | 5.340800 |
| | | | 1 | | 1.963674 | 1.963678 |
| | | | 1.5 | | 1.252943 | 1.252945 |
| | | | 2 | | 0.954249 | 0.954249 |
| | | | 2.5 | | 0.789781 | 0.789781 |
| | | | 1.5 | 0.5 | 1.763376 | 1.763372 |
| | | | | 2 | 1.366178 | 1.366179 |
| | | | | 4 | 1.177725 | 1.177725 |
| | | | | 6 | 1.079264 | 1.079264 |
| | | | | 8 | 1.014608 | 1.014608 |

Table 2: Variations of local heat transfer rate $\mathrm{Re}^{-1/2}\mathrm{Nu}_x$ for various values of $p_r$, $R_d$, $E_c$, $\theta_w$, and $\zeta_1$ at $n = 0.5$ and $n = 1.5$.

| Parameters | | | | | $\mathrm{Re}^{-1/2}\mathrm{Nu}_x$ | |
|---|---|---|---|---|---|---|
| $p_r$ | $R_d$ | $E_c$ | $\theta_w$ | $\zeta_1$ | $n = 0.5$ | $n = 1.5$ |
| 0.5 | 0.4 | 0.3 | 1.2 | 0.3 | 0.102894 | 0.189184 |
| 1 | | | | | 0.168418 | 0.292977 |
| 1.5 | | | | | 0.284903 | 0.347547 |
| 2 | | | | | 0.344818 | 0.376245 |
| 1.5 | 0.2 | | | | 0.257973 | 0.290954 |
| | 0.6 | | | | 0.291301 | 0.396726 |
| | 0.8 | | | | 0.279894 | 0.438540 |
| | 0.4 | 0.2 | | | 0.287578 | 0.352154 |
| | | 0.4 | | | 0.282224 | 0.342942 |
| | | 0.8 | | | 0.271514 | 0.324540 |
| | | 0.3 | 0.8 | | 0.219971 | 0.254794 |
| | | | 1 | | 0.246961 | 0.292226 |
| | | | 1.4 | | 0.331077 | 0.423023 |
| | | | 1.2 | 0.2 | 0.223443 | 0.257210 |
| | | | | 0.4 | 0.328880 | 0.420800 |
| | | | | 0.6 | 0.386372 | 0.531350 |

Table 3: Variations of local mass transfer rate $\mathrm{Re}^{-1/2}\mathrm{Sh}_x$ for various values of $N_b$, $N_t$, $\gamma$, Sc, and $p_r$ at $n = 0.5$ and $n = 1.5$

| Parameters | | | | | $\mathrm{Re}^{-1/2}\mathrm{Sh}_x$ | |
|---|---|---|---|---|---|---|
| $N_b$ | $N_t$ | $\gamma$ | Sc | $p_r$ | $n = 0.5$ | $n = 1.5$ |
| 0.1 | 0.1 | 0.3 | 0.5 | 1.5 | 0.168461 | 0.205503 |
| 0.2 | | | | | 0.084231 | 0.102752 |
| 0.3 | | | | | 0.056153 | 0.068501 |
| 0.2 | 0.2 | | | | 0.166745 | 0.205073 |
| | 0.3 | | | | 0.247369 | 0.306952 |
| | 0.4 | | | | 0.325899 | 0.403757 |

Table 3: Continued.

| Parameters | | | | | $\mathrm{Re}^{-1/2}\mathrm{Sh}_x$ | |
|---|---|---|---|---|---|---|
| $N_b$ | $N_t$ | $\gamma$ | Sc | $p_r$ | $n = 0.5$ | $n = 1.5$ |
| | 0.1 | 0.5 | | | 0.084212 | 0.102746 |
| | | 0.8 | | | 0.084176 | 0.102735 |
| | | 1 | | | 0.084153 | 0.102727 |
| | | 0.3 | 0.8 | | 0.084080 | 0.102689 |
| | | | 1 | | 0.084014 | 0.102658 |
| | | | 1.2 | | 0.083962 | 0.102633 |
| | | | 0.5 | 0.5 | 0.030420 | 0.055932 |
| | | | | 1 | 0.049792 | 0.086618 |
| | | | | 2 | 0.101942 | 0.111276 |
| | | | | 3 | 0.117134 | 0.121000 |

Table 3 demonstrates the mass transfer rate response for various values of parameters $N_b$, $N_t$, $\gamma$, Sc, and $p_r$. For both behaviors, the rise in $N_t$ and $p_r$ encouraged the mass transfer rate, as opposed to the parameters $N_b$, $\gamma$, and Sc.

## 5. Conclusion and Future Directions

In the present work, we have numerically analyzed the boundary layer incompressible MHD Carreau nanofluid flow above an extending sheet under the effect of nonlinear thermal radiation, Joule heating, heat absorption/generation, chemical reaction, and Darcy–Forchheimer law with the incorporation of thermophoresis and Brownian motion, issuing shear-thinning and thickening behavior. The continuation technique in the MATLAB bvp4c algorithm has been utilized to obtain numerical results. The findings of this study are summarized as follows:

(1) Increasing $M$ strengthens thermal and concentration boundary layers, while in contrast, the momentum boundary layer is decayed.

(2) As the Weissenberg number scales up, the velocity field for shear-thickening, the temperature and concentration fields for the shear-thinning case advance. On the other hand, the rise in this parameter results in a reverse effect on the velocity curve for the shear-thinning case and on the temperature and concentration profiles for the shear-thickening case.

(3) The rise in porosity and local inertia coefficient parameter penalizes the velocity field.

(4) An increment in $R_d$ from 0.1 to 0.4 lifted wall temperature by 20.62% at $n = 1.5$ and by 46.76% at $n = 0.5$.

(5) Increasing the values of $p$, $\theta_w$, $\zeta_1$, and $\omega$ uplifts temperature distribution. On the contrary, an increase in $P_r$ diminishes this profile.

(6) The concentration field is decayed by the rising value on $N_b$, Sc, and $\gamma$, whereas a rise in $N_t$ encouraged this profile.

(7) It is witnessed that increasing $E_c$ from 0 to 1.5, the average rise in temperature is 70.1% for shear-thickening fluid and 21.76% for shear-thinning fluid.

(8) By increasing thermophoresis from 0.1 to 0.4, the average rise in boundary layer temperature is 1.46% at $n = 1.5$ and 21.84% at $n = 0.5$.

(9) When the values of $M$, $p$, and $\alpha$ are uplifted, wall friction aggravates. The opposite result is achieved by surging the values of $n$ and $W_e$.

In our current work, we have employed the Fourier heat flux model and ignored the induced magnetic field. Nonetheless, in numerous empirical endeavors, such as high-temperature plasma, power generation, and purification of crude oil, the induced magnetic field effect plays a vital role. In future investigation, this problem can be extended for hybrid and trihybrid Carreau nanofluid convection and bio-convection by considering the induced magnetic field as well as the Cattaneo–Christov heat flux model.

## Nomenclature

$u$, $v$: Velocity components $(\mathrm{ms}^{-1})$
$x$, $y$: Space coordinates $(m)$
$a$: Stretching constant
$n$: Power-law index
$B_0$: Magnetic field $(\mathrm{kgk}^{-1}\mathrm{s}^{-1})$
$C$: Nanoparticle concentration
$T$: Fluid temperature $(k)$
$T_w$: Wall temperature of the fluid $(k)$
$D_B$: Brownian diffusion coefficient $(m^2 s^{-1})$
$Q_a$: Uniform volumetric heat source/sink
$N_b$: Brownian motion parameter
$T_\infty$: Free stream temperature $(k)$
$f_c$: Forchheimer coefficient
$p_m$: Permeability of porous medium
$N_t$: Thermophoresis parameter
$\mathrm{Re}_x$: Local Reynolds number
$R_d$: Radiation parameter
$D_T$: Thermophoresis diffusion coefficient $(m^2 s^{-1})$
$\theta_w$: Temperature ratio

$\mathrm{Nu}_x$: Local Nusselt number
Sc: Schmidt number
$k$: Thermal conductivity $(\mathrm{Wm}^{-1}k^{-1})$
$P_r$: Prandtl number
$W_e$: Weissenberg number
$E_c$: Eckert number
$q_r$: Radiative heat flux $(\mathrm{Wm}^{-2})$
$\mathrm{Sh}_x$: Local Sherwood number.

*Greek Letters*

$\nu$: Kinematic viscosity $(m^2s^{-1})$
$\alpha$: Local inertia coefficient $(m^2s^{-1})$
$\eta$: Similarity variable
$\lambda$: Time constant
$\tau$: Heat capacity ratio
$\rho_f$: Fluid density $(\mathrm{kgm}^{-3})$
$\beta_1$: Porosity of the medium $(m^2)$
$\gamma$: Chemical reaction parameter
$\omega$: Heat source/sink parameter
$\psi$: Stream function $(m^2s^{-1})$
$\zeta_1$: Heat transfer Biot number
$\sigma^*$: Stefan–Boltzmann constant $(\mathrm{Wm}^{-2}k^{-4})$
$\theta$: Dimensionless temperature
$\phi$: Dimensionless concentration
$\sigma_e$: Electrical conductivity.

*Abbreviations*

ODE: Ordinary differential equation
MHD: Magnetohydrodynamics
Eq: Equation
Ref: Reference
2D, 3D: Two dimension, three dimension
Pr: Present
e.g.: Example.

## Data Availability

The data used to support the findings of this investigation are incorporated in this article.

## Conflicts of Interest

The authors declare that they have no conflicts of interest with regard to the publication of this article.

## Acknowledgments

We express our heartfelt thankfulness to the authors of the literature used in this paper for the provided scientific aspects and ideas that support this work.

## References

[1] A. Subhas and P. Veena, "Visco-elastic fluid flow and heat transfer in a porous medium over a stretching sheet," *International Journal of Non-Linear Mechanics*, vol. 33, no. 3, pp. 531–540, 1998.
[2] H. Xu and S. J. Liao, "Laminar flow and heat transfer in the boundary-layer of non-Newtonian fluids over a stretching flat sheet," *Computers and Mathematics with Applications*, vol. 57, no. 9, pp. 1425–1431, 2009.
[3] A. Tamayol, K. Hooman, and M. Bahrami, "Thermal analysis of flow in a porous medium over a permeable stretching wall," *Transport in Porous Media*, vol. 85, no. 3, pp. 661–676, 2010.
[4] N. A. Khan and H. Khan, "A boundary layer flows of non-Newtonian Williamson fluid," *Nonlinear Engineering*, vol. 3, no. 2, pp. 107–115, 2014.
[5] S. U. S. Choi and J. A. Eastman, "Enhancing thermal conductivity of fluids with nanoparticles," *Journal of Advanced Sciences and Mathematics Education*, vol. 231, pp. 99–106, 1995.
[6] G. K. Ramesh, B. J. Gireesha, and C. S. Bagewadi, "MHD flow of a dusty fluid near the stagnation point over a permeable stretching sheet with non-uniform source/sink," *International Journal of Heat and Mass Transfer*, vol. 55, no. 17-18, pp. 4900–4907, 2012.
[7] J. Bouslimi, M. A. Abdelhafez, A. M. Abd-Alla, S. M. Abo-Dahab, and K. H. Mahmoud, "MHD mixed convection nanofluid flow over convectively heated nonlinear due to an extending surface with Soret effect," *Complexity*, vol. 2021, Article ID 5592024, 20 pages, 2021.
[8] B. Jalili, N. Aghaee, P. Jalili, and D. Domiri Ganji, "Novel usage of the curved rectangular fin on the heat transfer of a double-pipe heat exchanger with a nanofluid," *Case Studies in Thermal Engineering*, vol. 35, Article ID 102086, 2022.
[9] P. Jalili, A. Sadeghi Ghahare, B. Jalili, and D. Domiri Ganji, "Analytical and numerical investigation of thermal distribution for hybrid nanofluid through an oblique artery with mild stenosis," *SN Applied Sciences*, vol. 5, no. 4, p. 95, 2023.
[10] M. G. Reddy, "Influence of magnetohydrodynamic and thermal radiation boundary layer flow of a nanofluid past a stretching sheet," *Journal of Scientific Research*, vol. 6, no. 2, pp. 257–272, 2014.
[11] M. R. Krishnamurthy, B. Prasannakumara, B. J. Gireesha, and R. S. R. Gorla, "Effect of chemical reaction on MHD boundary layer flow and melting heat transfer of Williamson nanofluid in porous medium," *Engineering Science and Technology, an International Journal*, vol. 19, no. 1, pp. 53–61, 2016.
[12] A. C. Venkata Ramudu, K. Anantha Kumar, V. Sugunamma, and N. Sandeep, "Heat and mass transfer in MHD Casson nanofluid flow past a stretching sheet with thermophoresis and Brownian motion," *Heat Transfer*, vol. 49, no. 8, pp. 5020–5037, 2020.
[13] S. A. Abdollahi, P. Jalili, B. Jalili et al., "Computer simulation of Cu: AlOOH/water in a microchannel heat sink using a porous media technique and solved by numerical analysis AGM and FEM," *Theoretical and Applied Mechanics Letters*, vol. 13, Article ID 100432, 2023.
[14] A. Ishak, R. Nazar, and I. Pop, "Hydromagnetic flow and heat transfer adjacent to a stretching vertical sheet," *Heat and Mass Transfer*, vol. 44, no. 8, pp. 921–927, 2008.
[15] J. Bouslimi, M. Omri, R. A. Mohamed, K. H. Mahmoud, S. M. Abo-Dahab, and M. S. Soliman, "MHD Williamson nanofluid flow over a stretching sheet through a porous medium under effects of joule heating, nonlinear thermal radiation, heat generation/absorption, and chemical reaction," *Advances in Mathematical Physics*, vol. 2021, Article ID 9950993, 16 pages, 2021.
[16] M. Khan, M. Azam, and A. S. Alshomrani, "Effects of melting and heat generation/absorption on unsteady Falkner-Skan flow of Carreau nanofluid over a wedge," *International Journal of Heat and Mass Transfer*, vol. 110, pp. 437–446, 2017.

[17] N. A. Che Ghani and Z. Siri, "MHD flow of Carreau nanofluid over a stretching surface with suction/injection and slip effects by using Haar wavelet quasilinearization method," *Journal of Physics: Conference Series*, vol. 1139, no. 1, Article ID 012073, 2018.
[18] K. S. Babu, A. Parandhama, and R. B. Vijaya, "Non-linear MHD convective flow of Carreau nanofluid over an exponentially stretching surface with activation energy and viscous dissipation," *SN Applied Sciences*, vol. 3, no. 3, p. 382, 2021.
[19] N. G. Rudraswamy, S. A. Shehzad, K. Ganesh Kumar, and B. J. Gireesha, "Numerical analysis of MHD three-dimensional Carreau nanoliquid flow over bidirectionally moving surface," *Journal of the Brazilian Society of Mechanical Sciences and Engineering*, vol. 39, no. 12, pp. 5037–5047, 2017.
[20] T. Hayat, S. Qayyum, A. Alsaedi, and A. Shafiq, "Theoretical aspects of Brownian motion and thermophoresis on nonlinear convective flow of magneto Carreau nanofluid with Newtonian conditions," *Results in Physics*, vol. 10, pp. 521–528, 2018.
[21] R. M. A. Muntazir, M. Mushtaq, and K. Jabeen, "A numerical study of MHD Carreau nanofluid flow with gyrotactic microorganisms over a plate, wedge and stagnation point," *Mathematical Problems in Engineering*, vol. 2021, Article ID 5520780, 22 pages, 2021.
[22] R. A. Mohamed, S. M. Abo-Dahab, and M. S. Soliman, "Effects of nonlinear thermal radiation and heat generation/absorption on magnetohydrodynamic (MHD) Carreau nanofluid flow on a nonlinear stretching surface through a porous medium," *Journal of Nanofluids*, vol. 11, no. 6, pp. 845–856, 2022.
[23] J. Buongiorno, "Convective transport in nanofluids," *Journal of Heat Transfer*, vol. 128, no. 3, pp. 240–250, 2006.
[24] Z. Haddad, E. Abu-Nada, H. F. Oztop, and A. Mataoui, "Natural convection in nanofluids: are the thermophoresis and Brownian motion effects significant in nanofluid heat transfer enhancement?" *International Journal of Thermal Sciences*, vol. 57, pp. 152–162, 2012.
[25] M. Irfan, "Study of Brownian motion and thermophoretic diffusion on non-linear mixed convection flow of Carreau nanofluid subject to variable properties," *Surfaces and Interfaces*, vol. 23, Article ID 100926, 2021.
[26] A. Majeed, M. Zubair, A. Khan, T. Muhammad, and M. S. Alqarni, "Significance of thermophoretic and brownian motion on mhd nanofluids flow towards a circular cylinder under the inspiration of multiple slips: an industrial application," *Mathematical Problems in Engineering*, vol. 2021, Article ID 8634185, 14 pages, 2021.
[27] P. Jalili, H. Narimisa, B. Jalili, A. Shateri, and D. D. Ganji, "A novel analytical approach to micro-polar nanofluid thermal analysis in the presence of thermophoresis, Brownian motion and Hall currents," *Soft Computing*, vol. 27, no. 2, pp. 677–689, 2023.
[28] P. Jalili, H. Narimisa, B. Jalili, and D. D. Ganji, "Micro-polar nanofluid in the presence of thermophoresis, hall currents, and Brownian motion in a rotating system," *Modern Physics Letters B*, vol. 37, no. 01, 2023.
[29] C. Sulochana, G. P. Ashwinkumar, and N. Sandeep, "Transpiration effect on stagnation-point flow of a Carreau nanofluid in the presence of thermophoresis and Brownian motion," *Alexandria Engineering Journal*, vol. 55, no. 2, pp. 1151–1157, 2016.
[30] A. S. Mittal and H. R. Patel, "Influence of thermophoresis and Brownian motion on mixed convection two dimensional MHD Casson fluid flow with non-linear radiation and heat generation," *Physica A: Statistical Mechanics and Its Applications*, vol. 537, Article ID 122710, 2020.
[31] M. Imran, U. Farooq, T. Muhammad, S. U. Khan, and H. Waqas, "Bioconvection transport of Carreau nanofluid with magnetic dipole and nonlinear thermal radiation," *Case Studies in Thermal Engineering*, vol. 26, Article ID 101129, 2021.
[32] J. H. Merkin, "A model for isothermal homogeneous-heterogeneous reactions in boundary layer flow," *Mathematical and Computer Modelling*, vol. 24, no. 8, pp. 125–136, 1996.
[33] I. Khan, M. Y. Malik, T. Salahuddin, M. Khan, and K. U. Rehman, "Homogenous–heterogeneous reactions in MHD flow of Powell–Eyring fluid over a stretching sheet with Newtonian heating," *Neural Computing and Applications*, vol. 30, no. 11, pp. 3581–3588, 2018.
[34] S. Shaw, P. K. Kameswaran, and P. Sibanda, "Homogeneous-heterogeneous reactions in micro polar fluid flow from a permeable stretching or shrinking sheet in a porous medium," *Boundary Value Problems*, vol. 2013, no. 1, pp. 1–10, 2013.
[35] T. Hayat, M. Waqas, S. A. Shehzad, and A. Alsaedi, "On 2D stratified flow of an Oldroyd-B fluid with chemical reaction: an application of non-Fourier heat flux theory," *Journal of Molecular Liquids*, vol. 223, no. 1, pp. 566–571, 2016.
[36] B. J. Gireesha, P. S. Kumar, B. Mahanthesh, S. A. Shehzad, and A. Rauf, "Nonlinear 3D flow of Casson-Carreau fluids with homogeneous-heterogeneous reactions: a comparative study," *Results in Physics*, vol. 7, pp. 2762–2770, 2017.
[37] M. Gholinia, K. Hosseinzadeh, H. Mehrzadi, D. D. Ganji, and A. A. Ranjbar, "Investigation of MHD Eyring–Powell fluid flow over a rotating disk under effect of homogeneous–heterogeneous reactions," *Case Studies in Thermal Engineering*, vol. 13, Article ID 100356, 2019.
[38] B. Jalili, A. Rezaeian, P. Jalili, D. D. Ganji, and Y. Khan, "Squeezing flow of Casson fluid between two circular plates under the impact of solar radiation," *ZAMM- Journal of Applied Mathematics and Mechanics*, vol. 103, no. 9, Article ID e202200455, 2023.
[39] J. K. Zhang, B. W. Li, H. Dong, X. H. Luo, and H. Lin, "Analysis of magnetohydrodynamics (MHD) natural convection in 2D cavity and 3D cavity with thermal radiation effects," *International Journal of Heat and Mass Transfer*, vol. 112, pp. 216–223, 2017.
[40] S. Shaw, S. S. Samantaray, A. Misra, M. K. Nayak, and O. D. Makinde, "Hydromagnetic flow and thermal interpretations of Cross hybrid nanofluid influenced by linear, nonlinear and quadratic thermal radiations for any Prandtl number," *International Communications in Heat and Mass Transfer*, vol. 130, Article ID 105816, 2022.
[41] M. Irfan, A. Nadeem, N. Nasir, M. Waqas, and W. A. Khan, "Thermal phenomenon of Joule heating in the radiative flow of Carreau nanofluid," *Pramana*, vol. 96, no. 2, p. 90, 2022.
[42] P. Jalili, A. Ahmadi Azar, B. Jalili, Z. Asadi, and D. Domiri Ganji, "Heat transfer analysis in cylindrical polar system with magnetic field: a novel Hybrid Analytical and Numerical Technique," *Case Studies in Thermal Engineering*, vol. 40, Article ID 102524, 2022.
[43] T. Hayat, M. Hussain, S. Nadeem, and S. Mesloub, "Falkner–Skan wedge flow of a power-law fluid with mixed convection and porous medium," *Computers and Fluids*, vol. 49, no. 1, pp. 22–28, 2011.

[44] G. Rasool and T. Zhang, "Darcy-Forchheimer nanofluidic flow manifested with Cattaneo-Christov theory of heat and mass flux over non-linearly stretching surface," *PLoS ONE*, vol. 14, no. 8, Article ID e0221302, 2019.

[45] A. K. Alzahrani, M. Z. Ullah, A. S. Alshomrani, and T. Gul, "Hybrid nanofluid flow in a Darcy-Forchheimer permeable medium over a flat plate due to solar radiation," *Case Studies in Thermal Engineering*, vol. 26, Article ID 100955, 2021.

[46] M. K. Siddiq, M. Ashraf, and T. Mushtaq, "MHD thermally radiative flow of Carreau fluid subjected to the stretching sheet by considering non-Darcy Forchheimer law," *Pramana*, vol. 95, no. 164, pp. 1–9, 2021.

[47] P. J. Carreau, "Rheological equations from molecular network theories," *Transactions of the Society of Rheology*, vol. 16, no. 1, pp. 99–127, 1972.

[48] M. Khan and Hashim, "Boundary layer flow and heat transfer to Carreau fluid over a nonlinear stretching sheet," *AIP Advances*, vol. 5, no. 10, Article ID 107203, 2015.

[49] G. R. Machireddy and S. Naramgari, "Heat and mass transfer in radiative MHD Carreau fluid with cross diffusion," *Ain Shams Engineering Journal*, vol. 9, no. 4, pp. 1189–1204, 2018.

[50] S. M. Roberts and J. S. Shipman, "Continuation in shooting methods for two-point boundary value problems," *Journal of Mathematical Analysis and Applications*, vol. 18, no. 1, pp. 45–58, 1967.